Catal Lett (2012) 142:637–645
DOI 10.1007/s10562-012-0785-5

Preparation and Improved Photocatalytic Activity of $WO_3 \cdot 0.33H_2O$ Nanonetworks

Xiaoyu He · Chenguo Hu · Qianning Yi · Xue Wang · Hao Hua · Xiaoyan Li

Received: 27 December 2011 / Accepted: 13 February 2012 / Published online: 7 March 2012

Abstract Multi-structural tungsten oxide ($WO_3 \cdot 0.33H_2O$) samples were prepared using a hydrothermal method in the presence of different salts Na_2SO_4 and $CaCl_2$ respectively. The experimental results showed that pH value of the reaction solution greatly affects crystal morphology of the final products. To explore the photocatalysis originated from nanonetwork hierarchical structure, the photodegradation of methylene blue was carried out under simulated sunlight irradiation. The photocatalytic activity of the $WO_3 \cdot 0.33H_2O$ nanonetworks was compared with that of the nanoplates, and the former showed a higher photocatalytic activity owing to its novel hierarchical structure. Our investigation demonstrates that nanonetwork hierarchical structure can promote sunlight absorption due to higher specific surface area.

Keywords Tungsten oxide · Nanostructures · Hydrothermal synthesis · Photocatalysis

1 Introduction

It is well known that the physical and chemical properties of most materials are strongly dependent on their shapes and structures. Therefore, controlling the shape of the materials is always one of the most challenging work for inorganic chemists and material specialists. Recently, complex three-dimensional (3D) nanoarchitectures have attracted much attention since such architectures possess features of micrometer and nanometer-scaled building blocks and novel properties to be explored [1, 2].

Materials based on tungsten oxide, including tungsten oxides (WO_{3-x}) and tungsten oxide hydrates ($WO_3 \cdot nH_2O$), have been studied extensively because of their special electronic and optoelectronic properties, which have enormous potential applications in the fields ranging from condensed-matter physics to solid-state chemistry[3], such as photo-electrochemical energy conversion [4], gas-sensors [5], photo-catalysts [6], lithium-ion batteries [7], solar cells [8], electron emitters [9], optical storage media [10]. Crystalline tungsten oxide and tungsten oxide hydrates have been synthesized previously [11–15]. Among the hydrates, the structures of $WO_3 \cdot 2H_2O$, $WO_3 \cdot H_2O$ and $WO_3 \cdot 0.33H_2O$ have been well documented. In particular, $WO_3 \cdot 0.33H_2O$ was first prepared by Gerand et al. [16], and they obtained the micrometer sized platelets and nanoneedle aggregates by hydrothermal treatment of aqueous suspension of either tungstic acid gel (prepared by acidification of sodium tungstate) or crystallized $WO_3 \cdot 2H_2O$ at 120 °C. Further studies revealed that the $WO_3 \cdot 0.33H_2O$ phase could also be obtained by the thermal decomposition of titanium or vanadium containing peroxo-polytungstic acid [17–19] or acid leaching of tungsten containing compounds such as $LiVWO_6$, $LiAlW_2O_8$, and $LiFeW_2O_8$ [20]. However, nanoscaled photocatalysts with control morphologies are hard to be achieved by these methods.

To improve the photocatalysis of tungsten oxide and tungsten oxide hydrate, several strategies can be adopted: phase and morphological control [21], surface sensitization, decorated with noble metals [22–28] or hybridized with TiO_2 nanostructures [29]. Interestingly, nanoscaled

X. He · C. Hu (✉) · Q. Yi · X. Wang · H. Hua · X. Li
Department of Applied Physics, Chongqing University, Chongqing 400044, People's Republic of China
e-mail: hucg@cqu.edu.cn

X. He
Department of Physics and Electronic Engineering, Yangtze Normal University, Chongqing 408100, People's Republic of China

photocatalysts with controlled morphology possess enhanced photocatalytic activities due to their novel morphology and large surface area. It has been demonstrated that flower-shaped hierarchical structure can provide a varied liquid pressure [30] and better absorption of sunlight [31]. We think the varied liquid pressure and enhanced absorption in the hierarchical or network structure might improve the photocatalysis. It is an interesting work to know whether the $WO_3{\cdot}0.33H_2O$ hierarchical or network structure should have high photocatalysis.

Herein, we have adopted a facile method to prepare 3D $WO_3{\cdot}0.33H_2O$ nanonetworks and two-dimensional nanoplates for the first time with the hydrothermal approach in which $CaCl_2$ and sodium sulfate (Na_2SO_4) were used as the structure-directing agents respectively. Our research revealed that a novel $WO_3{\cdot}0.33H_2O$ nanostructure can be produced via a traditional hydrothermal route. Morphology evolution mechanism of the products has been investigated. The photocatalytic activity of the $WO_3{\cdot}0.33H_2O$ nanonetworks and nanoplates was comparatively evaluated by photodegradation of methylene blue (MB) under the simulated sunlight irradiation.

2 Experimental

2.1 Preparation of $WO_3{\cdot}0.33H_2O$ Nanonetworks

All the chemicals were of analytical grade and used without further purification. In a typical process, sodium tungstate (Na_2WO_4) (0.4 mmol) and $CaCl_2$ (0.4 mmol) were firstly dissolved into distilled water (40 mL) in two beakers, respectively, then the nitric acid (HNO_3) (3 M) was slowly added into the two beakers until the pH value of the each solution reached 3.3. These two solutions were mixed and the mixture was transferred into a Teflon-lined stainless autoclave and heated at 180 °C for 24 h. After reaction, the autoclave was taken out and allowed cool to room temperature. The final product was obtained by centrifugation and washed with deionized water and pure alcohol to remove ions possibly remaining in the final product.

2.2 Preparation of $WO_3{\cdot}0.33H_2O$ Nanoplates

In a typical synthesis, the solution of 0.2 mmol Na_2WO_4 and 0.8 mmol Na_2SO_4 was prepared in a beaker with 20 mL of deionized water. Under stirring, an aqueous solution of HNO_3 (3 M) was added dropwise to the beaker until the pH value of the solution reached 1.3. The mixture was transferred into a Teflon-lined stainless autoclave and heated at 180 °C for 24 h. After reaction, the autoclave was taken out and allowed to cool at room temperature and then washed with distilled water.

2.3 Degradation of MB

The degradation of MB was performed in a beaker in exposure to the simulated sunlight at room temperature. 20 mg of the $WO_3{\cdot}0.33H_2O$ nanonetwork catalyst was dispersed in 80 mL of 10 mg/L MB aqueous solution. Prior to illumination, the suspensions were magnetically stirred in the dark for 30 min to ensure the establishment of adsorption–desorption equilibrium of MB on the surface of catalyst. Then, the measurement of photocatalytic reactivity was carried out using a simulated sunlight instrument (CH-XM-500 W) with intensity of 100 mW/cm^2. At given intervals, 3 mL of the suspension was extracted and then centrifuged at a rate of 2,000 rmp for 2 min to remove the catalyst. The concentration change of MB was then determined by using an UV–Visible Spectrophotometer (Hitachi U-4100). Analogous experiments were performed with $WO_3{\cdot}0.33H_2O$ nanoplates under the same condition.

2.4 Characterization

The structure and morphology of the as-prepared products were characterized with X-ray diffraction (XRD, BDX3200 with Cu Kα radiation), field emission scanning electron microscopy (FESEM, FEI Nova 400), transmission electron microscope (TEM, JEOL-4000EX). The UV–Visible spectra of the samples were recorded by an UV–Visible Spectrophotometer (Hitachi U-4100). The specific surface areas were calculated by a multipoint Brunauer–Emmett–Teller (BET) analysis of the nitrogen adsorption isotherms recorded on a surface area analyzer (Micromeritics ASAP 2020 M).

3 Results and Discussion

3.1 Characterization of $WO_3{\cdot}0.33H_2O$ Samples

The $WO_3{\cdot}0.33H_2O$ nanonetworks can be selectively prepared in the presence of $CaCl_2$. XRD pattern of the products obtained at 180 °C for 24 h in pH value 3.3 is shown in Fig. 1 pattern a. All the diffraction peaks can be indexed to the pure orthorhombic phase of $WO_3{\cdot}0.33H_2O$, which agree well with the data from the JCPDS card (35-0270). No peaks of impurities were detected from this pattern. The morphology and microstructures of the samples were shown by SEM and TEM images in Fig. 2. Fig. 2a and b show the high yield 3D networks with the average diameters around 5 μm. The selected area electron diffraction pattern shown in Fig. 2c indicates that the sheet of nanonetworks is made of single crystal morphology, for which the long axis corresponds to the [200] direction.

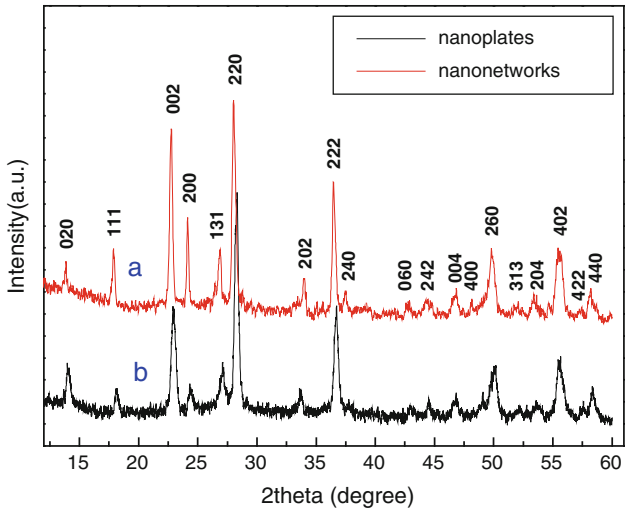

Fig. 1 XRD pattern of the $WO_3 \cdot 0.33H_2O$ nanonetworks (*pattern a*) and nanoplates (*pattern b*)

The spacing of the lattice fringes are found to be about 0.352 nm, as shown in Fig. 2d, which confirms that the sheet grows along [200] direction.

To investigate the growth process of the $WO_3 \cdot 0.33H_2O$ network structures, we conducted experiments at different pH values. Two obvious evolutionary stages could be clearly observed, as shown in Fig. 3. When the experiment was carried out at 180 °C for 24 h under different pH values, the morphology of the products varied dramatically, indicating that the pH value played a crucial role in the crystal growth process. When the experiment was conducted at low pH value (<2.5), irregular particles were obtained (Fig. 3a). A great deal of oval-shaped particles could easily be obtained when the reaction system was set in the pH range of 2.5–3.0 (Fig. 3b). As the pH value increased, uniform nanochips connected together in groups at their bases and self-assembled into the network-like morphology, as shown in Fig. 3c. Figure 3d is the magnified SEM image of the networks, which was synthesized at pH value 3.3.

The plate-like assemblies of $WO_3 \cdot 0.33H_2O$ can be selectively prepared in the presence of Na_2SO_4. XRD measurements of the powder shown in Fig. 1 pattern b, indicating that the sample is phase-pure orthorhombic

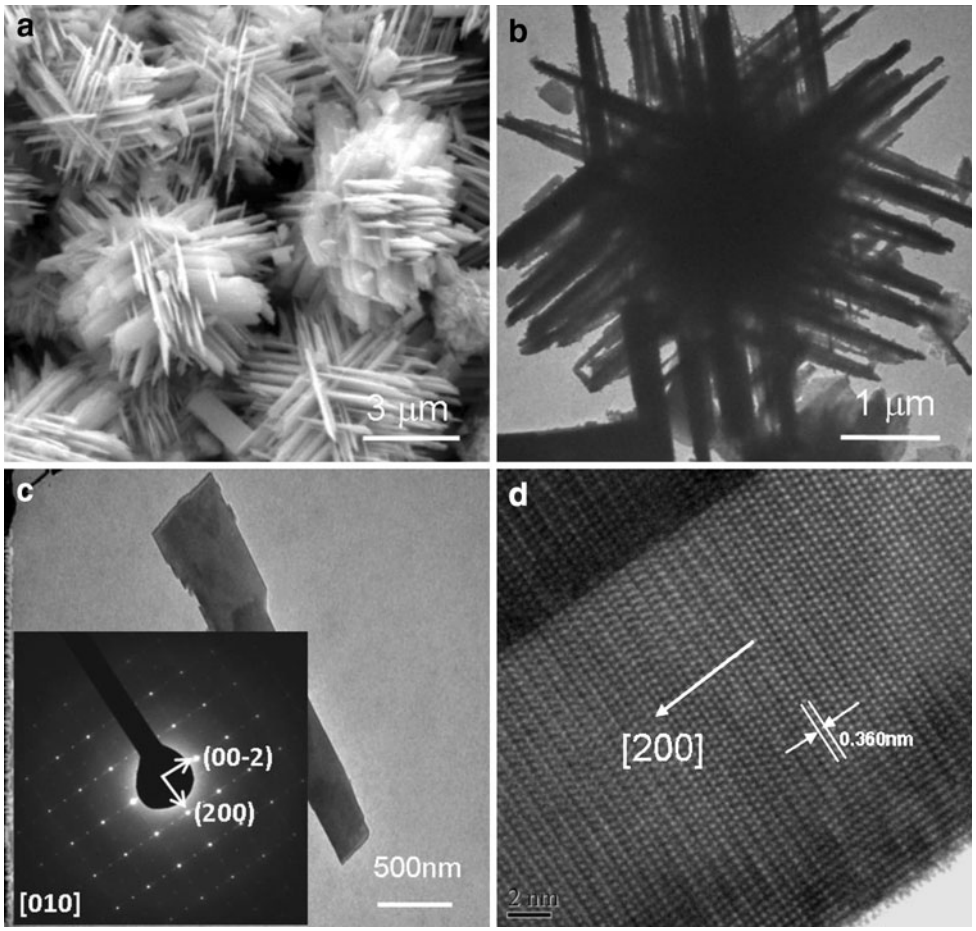

Fig. 2 SEM image (**a**), TEM images (**b**, **c**), SAED (*inset c*) and HRTEM image (**d**) of the $WO_3 \cdot 0.33H_2O$ networks obtained prepared in the presence of $CaCl_2$ at 180 °C, pH = 3.3, for 24 h

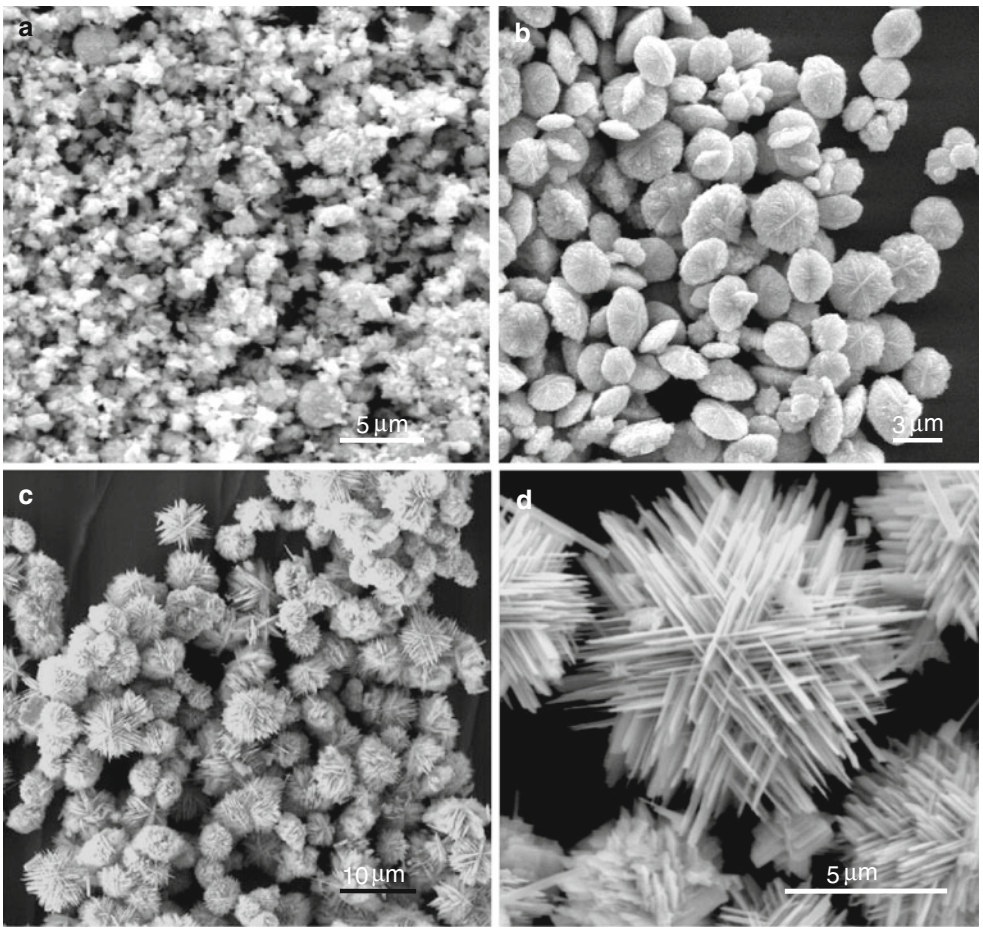

Fig. 3 SEM images of the $WO_3 \cdot 0.33H_2O$ samples synthesized in the presence of $CaCl_2$ at 180 °C for 24 h under different pH values pH < 2.5 (**a**), 2.5 < pH < 3 (**b**), pH = 3.3 (**c**)

structured $WO_3 \cdot 0.33H_2O$ which also agrees well with the data from the JCPDS card (35-0270). The SEM image of the as-synthesized products in Fig. 4a shows that the diameter of the sample is about 4 μm. The thickness of the plates is between 400 and 500 nm and the plate is covered by thousands of irregular nanorods, as is estimated from the Fig. 4b. The nanorod length ranges from 400 to 500 nm and the end is a part of hexagon observed from the edge in Fig. 4c, d. The selected area electron diffraction pattern taken from these nanorods are shown in Fig. 4d. Though the diffraction pattern is multi-diffraction spots taken from a few nanorods, it can indicate that the facet of the nanoplates is [−111] plane.

The pH value-dependent experiments were further carried out to investigate the growth process of the $WO_3 \cdot 0.33H_2O$ nanoplates at fixed temperature and growth time (180 °C, 24 h) under different pH values. When the experiment was conducted at high pH value (>2.3), no products were obtained. Nanorods could be easily obtained, when the reaction system was set in the pH range of 2.3–1.7 (Fig. 5a, b). From the diffraction pattern recorded from a nanorod (inset in Fig. 5b), the pattern clearly indicates that the nanorods grow along [002] direction. As the pH value decreased, the nanorods tended to aggregate, resulting in the formation of bundle structures (Fig. 5c). When the pH value was about 1.3, uniform plates were obtained (Fig. 5d). As the pH value decreased lower than 1.2, a large number of irregular columns appeared (Fig. 5e). The XRD pattern of the nanorods and irregular columns (Fig. 5f) still can be well indexed as the pure orthorhombic phase of $WO_3 \cdot 0.33H_2O$ (JCPDS 35-0270).

Based on the above experimental results, the mechanism for the formation of $WO_3 \cdot 0.33H_2O$ is speculated as follows:

$$Na_2WO_4 + 2HNO_3 + nH_2O \rightarrow H_2WO_4 \cdot nH_2O + 2NaNO_3 \quad (1)$$

$$3H_2WO_4 \cdot nH_2O \xrightarrow{Na_2SO_4/CaCl_2} 3WO_3 \cdot 0.33H_2O + (n + 2)H_2O. \quad (2)$$

To obtain $WO_3 \cdot 0.33H_2O$ products, some acid must be dropped in the mixture solution owing to the alkalinity of the Na_2WO_4 aqueous solution under hydrothermal conditions.

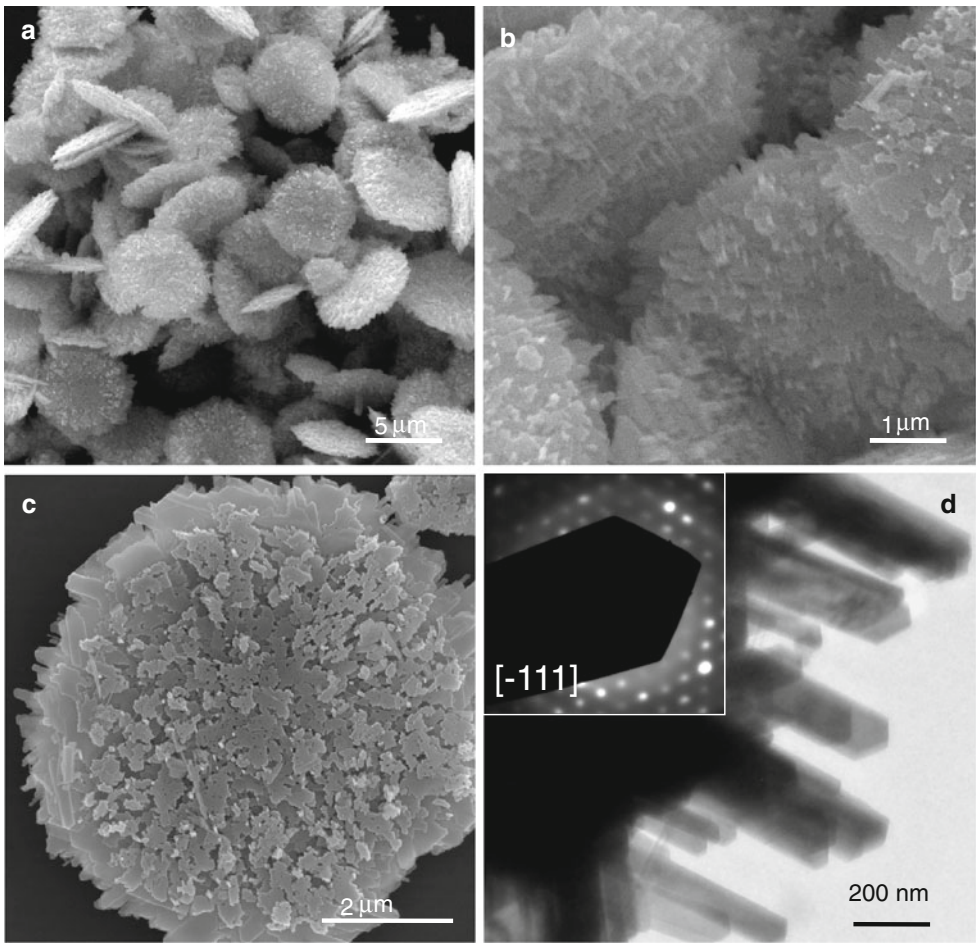

Fig. 4 SEM image (**a**), FESEM images (**b**, **c**), TEM image (**d**) and SAED of the edge of the nanoplate (*inset*) of the $WO_3 \cdot 0.33H_2O$ nanoplates obtained in the presence of Na_2SO_4 at 180 °C, pH 3.3, for 24 h

However, excessive acid may induce the formation of irregular structures. The very low pH value with high concentration of hydrogen ions in solution can lead to an extremely fast nucleation process to generate small, not well-defined nuclei, and then Cl^- or SO_4^{2-} ions may adsorb in large amounts onto all the facets of the nuclei without any selectivity. Those particles or short nanorods tend to aggregate in order to lower their surface energy, and finally the uneven morphologies are formed. Therefore, to obtain the desired crystal structure and morphology of the products, the pH value should be strictly controlled. Figure 6a, b summarize all major steps and changes involved in the formation of the $WO_3 \cdot 0.33H_2O$ nanonetworks and nanoplates respectively.

To better understand the morphological difference between the two $WO_3 \cdot 0.33H_2O$ nanonetworks and nanoplates, the BET analysis for surface area, pore size and volume was taken on the films made from the two samples. Though it is not the real situation in solution, but it can give a good assessment for comparing the two samples. The results are summarized in Table 1. The specific surface area of the $WO_3 \cdot 0.33H_2O$ nanonetworks is larger than that of the $WO_3 \cdot 0.33H_2O$ nanoplates from the BET analysis, indicating that the larger specific surface area of the $WO_3 \cdot 0.33H_2O$ nanonetworks due to the hierarchical structure.

3.2 Photocatalytic Activity

To explore the influence of microstructure on photocatalysis, photocatalytic activity of the $WO_3 \cdot 0.33H_2O$ nanonetworks was compared with that of the nanoplates. The photocatalytic activity of the $WO_3 \cdot 0.33H_2O$ nanostructure was evaluated with the photodegradation of MB in aqueous solution under irradiation of the simulated sunlight. Figure 7a, b show the UV–Visible absorption spectra of starting solution (10 mg/L MB) and the solution with 0.25 g/L $WO_3 \cdot 0.33H_2O$ nanonetworks for catalytic degradation. It can be seen that the concentration of MB decreases with the illumination time. The absorption peaks of MB almost disappeared after 7 h irradiation of the simulated sunlight by the photocatalysis of the $WO_3 \cdot 0.33H_2O$ nanonetworks, while 86% of MB was removed by the $WO_3 \cdot 0.33H_2O$ nanoplates, suggesting a better photocatalytic activity of the nanonetwork structure

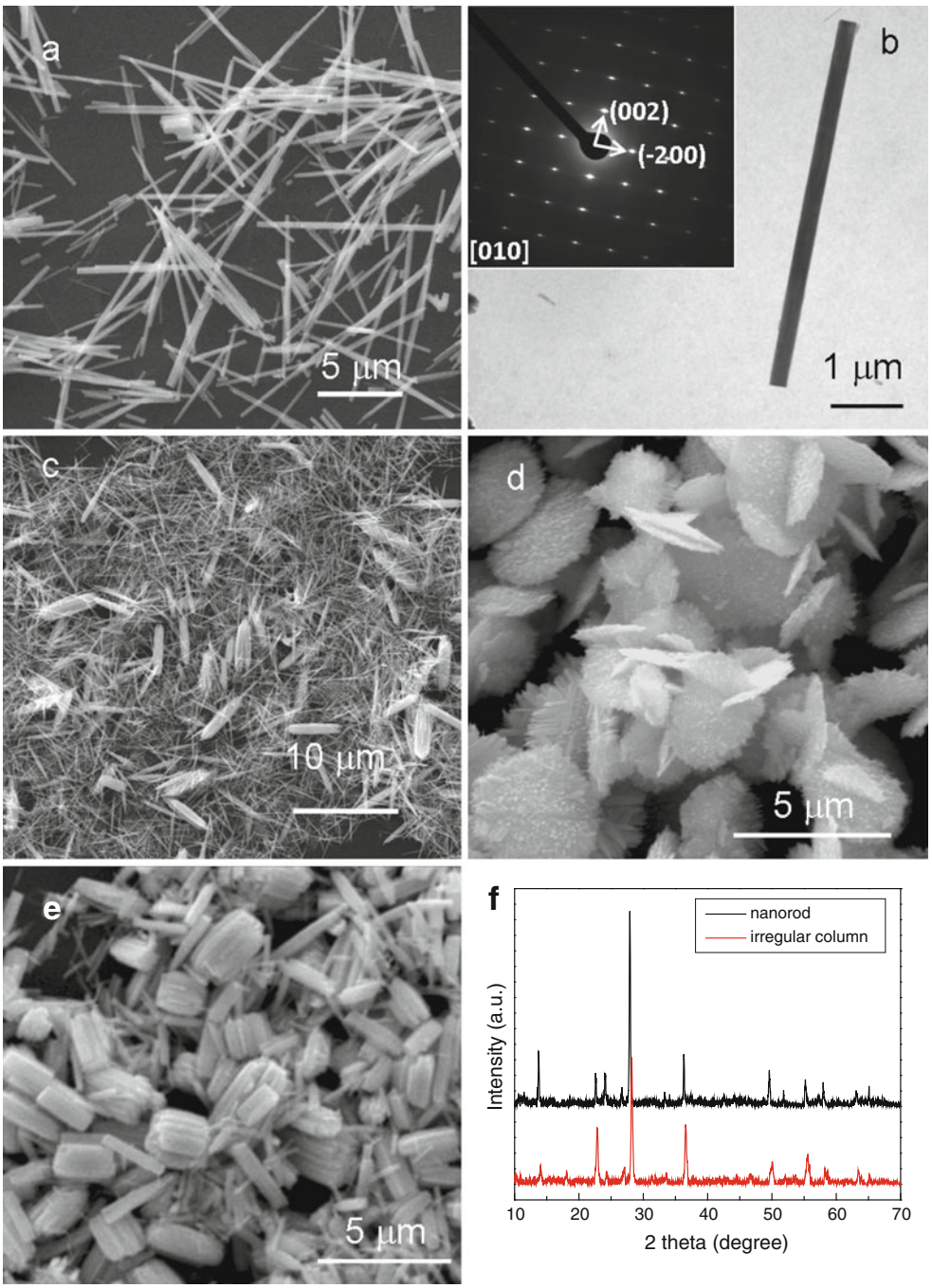

Fig. 5 Characterizations of samples prepared in the presence of Na_2SO_4.at 180 °C for 24 h under different pH values. SEM/TEM image of the sample obtained in 1.7 < pH < 2.3 (**a**, **b**), 1.4 < pH < 1.7 (**c**), pH = 1.3 (**d**) and pH < 1.2 (**e**). Diffraction pattern of a nanorod (*inset*). XRD patterns of the sample prepared at 1.7 < pH < 2.3 (*nanorods*) and pH < 1.2 (*irregular columns*) (**f**)

than that of the nanoplate structure. Figure 7c shows the plots of the catalytic degradation percentage versus illumination time, which indicates that after 1 h, the degradation percentage of the nanonetworks was higher than that of the nanoplates. The degradation without illumination in the early stage comes from adsorption of the dye on the catalysts.

3.3 Catalytic Mechanism

UV–Visible reflection spectrums of the $WO_3{\cdot}0.33H_2O$ nanonetworks are presented in Fig. 8, which shows a clear absorption edge at 3.2 eV, a little larger compared with that of the band gap for WO_3 (~2.8 eV) [32]. The band gap of $WO_3{\cdot}0.33H_2O$ indicates that the electron transition from

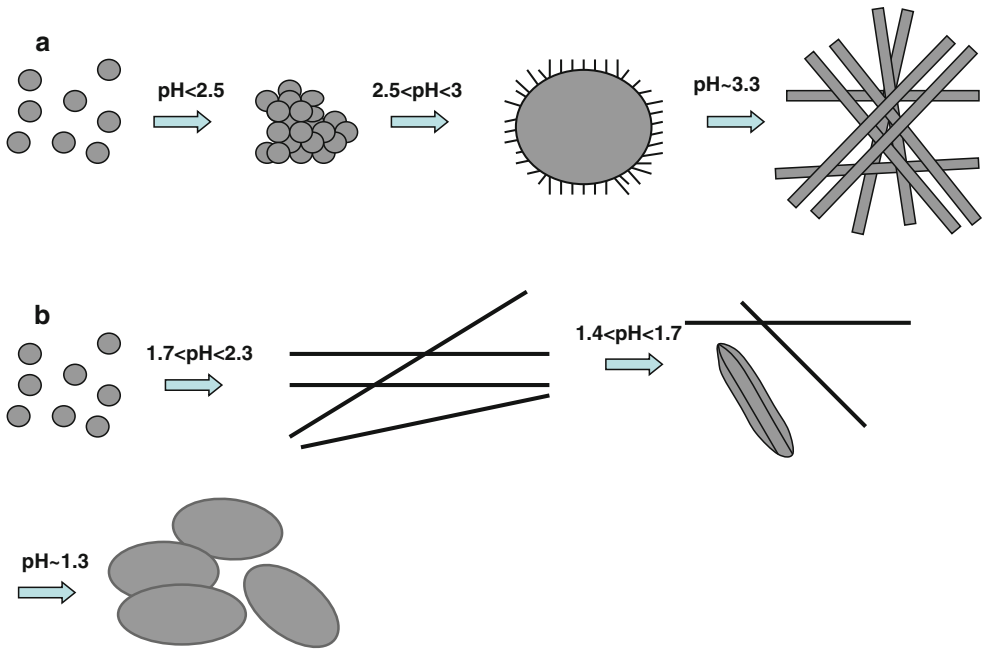

Fig. 6 Schematic illustration of the formation process of $WO_3 \cdot 0.33H_2O$ nanonetworks (**a**) and plates-like nanostructures (**b**)

Table 1 Results of the BET analysis

Sample	BET surface area (m^2/g)	Pore size (nm)	Pore volume (cm^3/g)
WO_3 nanonetworks	6. 5	8.9	0.09
WO_3 nanoplates	4.2	6.1	0.05

valence-band to conduction-band can only be excited by absorbing the energy of UV wavelength less than 387 nm. Though the percentage of UV-light in the simulated sunlight is very small (3–5%), photocatalytic activity was still obvious.

In order to explain the catalytic mechanism and compare the morphology-dependent light absorption ability, UV–Visible absorption spectra were measured by dispersing $WO_3 \cdot 0.33H_2O$ nanonetworks and nanoplates in ethanol with the same concentration (Fig. 9). We can see obvious band edge absorption is around 400 nm for these two samples. However, the absorbance plot of the $WO_3 \cdot 0.33H_2O$ nanonetworks is higher than that of the $WO_3 \cdot 0.33H_2O$ nanoplates, indicating the better absorption ability of the hierarchical structure of the nanonetworks. On the other hand, the unique network-shaped hierarchical structure can provide microchannels for reactant diffusion in which a varied liquid pressure can significantly reduce the liquid sealing effect [30]. It is well known that the larger specific surface area of catalysts can improve catalytic activity due to the less steric hindrance for the diffusion of reactants [33], and can provide a photocatalyst with more total active sites photocatalytic reactions.

The photocatalytic degradation by the $WO_3 \cdot 0.33H_2O$ nanocrystals under the sunlight irradiation can be explained as follows. When the $WO_3 \cdot 0.33H_2O$ photocatalysts were irradiated with the sunlight, photogenerated electron–hole pairs are produced. The electrons and holes react with the adsorbed surface substances, like O_2, OH^- etc., to form reactive species O_2^-, OH*, which is the major oxidative species for the decomposition of organic pollutants. Based on the above analysis, the photocatalytic reaction can be expressed as follows:

$$WO_3 \cdot 0.33H_2O + h\nu(E > E_g) \rightarrow WO_3 \cdot 0.33H_2O + e^- + h^+ \quad (1)$$

$$h^+ + H_2O \rightarrow OH^* + H^+, \quad (2)$$

$$h^+ + OH^- \rightarrow OH^* \quad (3)$$

$$O_2 + e^- \rightarrow O_2^- \quad (4)$$

$$2H_2O + O_2^- + e^- \rightarrow 2OH^* + 2OH^-, \quad (5)$$

$$OH^* + MB \rightarrow CO_2 + H_2O. \quad (6)$$

4 Conclusions

The 3D $WO_3 \cdot 0.33H_2O$ nanostructures have been prepared by the simple hydrothermal method in the presence of different salts. The pH value is found to be a crucial factor in determining the morphology of the final product due to the influence on the early nucleation process, and nanonetworks, nanoplates, nanoovals, nanoparticles and nanowires can be obtained by adjusting pH value. The photodegradation experiment indicates that $WO_3 \cdot 0.33H_2O$

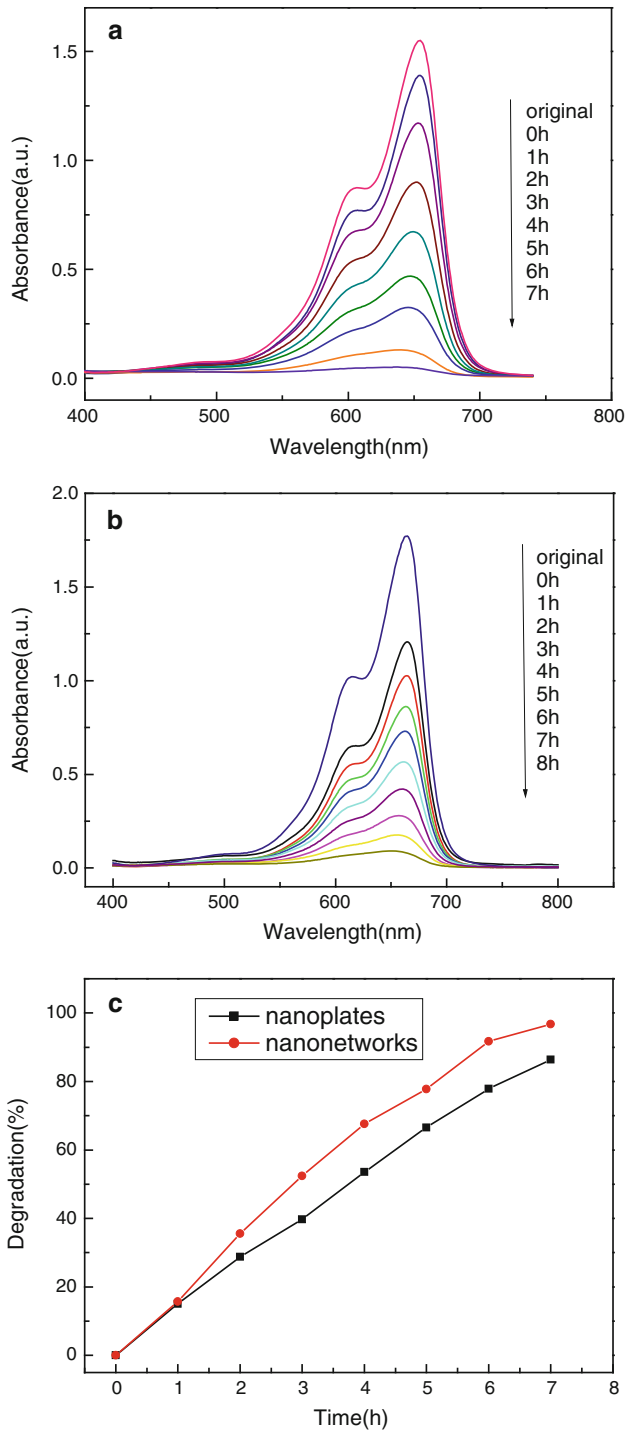

Fig. 7 Absorption spectrum of 10 mg/L MB solution with 0.25 g/L $WO_3 \cdot 0.33H_2O$ nanonetwoks (**a**) or nanoplates (**b**) in different stages under illumination of the simulated sunlight and the plot of degradation percentage versus illumination time (**c**)

nanonetworks exhibit better photocatalytic degradation of MB under the simulated sunlight irradiation than that of the $WO_3 \cdot 0.33H_2O$ nanoplates, which demonstrates the specific hierarchical structure can improve the light absorption and

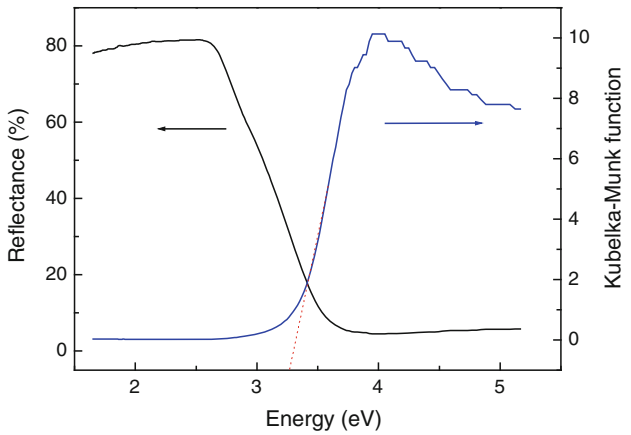

Fig. 8 UV–Vis reflection spectrum and Kubelka–Munk function of the $WO_3 \cdot 0.33H_2O$ nanonetworks

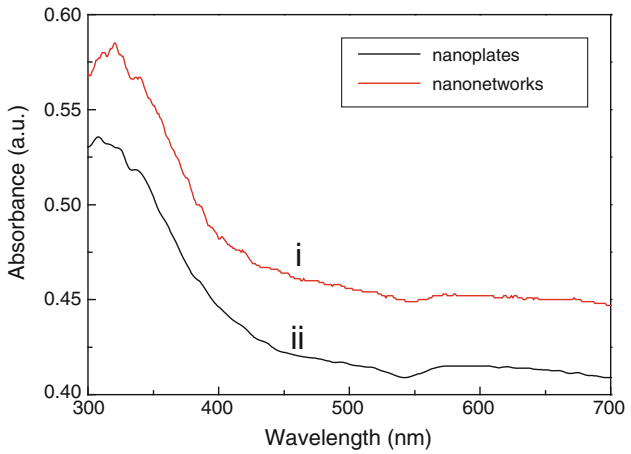

Fig. 9 UV–Visible absorption spectra of the $WO_3 \cdot 0.33H_2O$ nanonetworks (*i*) and nanoplates (*ii*)

provide higher specific surface area. The microchannels in the nanonetwork hierarchical structure can also promote reactant diffusion owing to the liquid sealing effect reduced by a varied liquid pressure in the channels. This investigation proves a very good catalyst structure based in $WO_3 \cdot 0.33H_2O$ nanonetworks.

Acknowledgments This work is supported by the NSFC (60976055), SRFDP (20110191110034), Project (WLYJSBJRCT D201101) of the Innovative Talent Funds for 985 Project, and the large-scaled equipment sharing fund of Chongqing University.

References

1. Lu F, Cai WP, Zhang YP (2008) Adv Funct Mater 18:1047
2. Li BX, Rong GX, Xie Y, Huang LF, Feng CQ (2006) Inorg Chem 45:6404
3. Zheng HD, Ou JZ, Strano MS, Kaner RB, Mitchell A, Kalantar-zadeh K (2011) Adv Funct Mater 21:2175

4. Higashimoto S, Kitahata N, Mori K, Azuma M (2005) Catal Lett 101:49
5. Kim YS, Ha SC, Kim K, Yang H, Choi SY, Kim YT, Park JT, Lee CH, Choi JY, Paek JS, Lee K (2005) Appl Phys Lett 86:213105
6. Yu CL, Yu JC, Zhou WQ, Yang K (2010) Catal Lett 140:172
7. Galiote NA, Huguenin F (2007) J Phys Chem C 111:14911
8. Zheng HD, Tachibana Y, Kalantar-zadeh K (2010) Langmuir 26:19148
9. Zhang XH, Gong L, Liu K, Chao YZ, Xiao X, Sun WM, Hu XJ, Gao YH, Chen J, Zhao J, Wang ZL (2010) Adv Mater 22:5292
10. Turyan I, Krasovec UO, Orel B, Saraidorov T, Reisfeld R, Mandler D (2000) Adv Mater 12:330
11. Yang B, Barnes PRF, Zhang YJ, Luca V (2007) Catal Lett 118:280
12. Gu ZJ, Zhai TY, Gao BF, Sheng XH, Wang YB, Fu HB, Ma Y, Yao JN (2006) J Phys Chem B 110:23829
13. Wang Z, Zhou S, Wu L (2007) Adv Funct Mater 17:1721
14. Zhou J, Ding Y, Deng SZ, Gong L, Xu NS, Wang ZL (2005) Adv Mater 17:2107
15. Yu JG, Yu HG, Guo HT, Li M, Mann S (2008) Small 4:87
16. Gerand B, Nowogrocki G, Figlarz M (1981) J Solid State Chem 383:12
17. Dupont L, Larcher D, Portemer D, Figlarz M (1996) J Solid State Chem 121:339
18. Yebka B, Pecquenard B, Julien C, Livage J (1997) Solid State Ion 104:169
19. Pecquenard B, Lecacheux H, Livage J, Julien C (1998) J Solid State Chem 135:159
20. Bhuvanesh NSP, Uma S, Subbanna GN, Gopalakrishnan J (1995) J Mater Chem 5:927
21. Hu DH, He YQ, Li LJ, Yin T, Ji LL (2011) Chin J Inorg Chem 27:11
22. Abe R, Takami H, Murakami N, Ohtani B (2008) J Am Chem Soc 130:7780
23. Arai T, Horiguchi M, Yanagida M, Gunji T, Sugihara H, Sayama K (2008) Chem Commun 435:565
24. Arai T, Yanagida M, Konishi Y, Iwasaki Y, Sugihara H, Sayama K (2007) J Phys Chem C 111:7574
25. Arai T, Yanagida M, Konishi Y, Iwasaki Y, Sugihara H, Sayama K (2008) Catal Commun 9:1254
26. Arai T, Yanagida M, Konishi Y, Sugihara H, Sayama K (2008) Electrochemistry 76:128
27. Arai T, Yanagida M, Konishi Y, Ikura A, Iwasaki Y, Sugihara H, Sayama K (2008) Appl Catal B Environ 84:42
28. Xiang Q, Meng GF, Zhao HB, Zhang Y, Li H, Ma WJ, Xu JQ (2010) J Phys Chem C 114:2049
29. Ke DN, Liu Hj, Peng TY, Liu X, Dai K (2008) Mater Lett 62:447
30. Xie FY, Tian ZQ, Meng H, Shen PK (2005) J Power Sources 141:211
31. Zhang HL, Hu CG (2011) Catal Commun 14:32
32. Sun SM, Wang WZ, Zeng SZ, Shang M (2010) J Hazard Mater 178:427
33. Wang QQ, Lin BZ, Xu BH, Li XL, Chen ZJ, Pian XT (2010) Microporous Mesoporous Mater 130:344